

# SIMULATION OF MICROLOADING AND ARDE IN DRIE

M.A. Gosalvez<sup>1,2,3</sup>, Y. Zhou<sup>4</sup>, Y. Zhang<sup>4</sup>, G. Zhang<sup>5</sup>, Y. Li<sup>5</sup> and Y. Xing<sup>5</sup>

<sup>1</sup>Dept. of Materials Physics, Univ. of the Basque Country UPV/EHU, San Sebastian, Spain

<sup>2</sup>Centro de Física de Materiales (centro mixto CSIC – UPV/EHU), San Sebastian, Spain

<sup>3</sup>Donostia International Physics Center (DIPC), San Sebastian, Spain

<sup>4</sup>IntelliSense Corp., Nanjing High-Tech Zone, Nanjing, China

<sup>5</sup>Micro-Nano Medical Devices Lab., Dept. of Mech. Eng., Southeast University, Nanjing, China

## ABSTRACT

An atomistic etching model is combined with a continuum concentration solver in order to realistically simulate various effects during Deep Reactive Ion Etching (DRIE or the Bosch process). This includes microloading (or loading effect) and Aspect Ratio Dependent Etching (ARDE or lag effect). The model strongly differs from the current simulation approaches in which the local etch rate depends markedly on complex visibility integrals over the ion and neutral fluxes. Instead, we focus on the description of the etchant depletion.

## KEYWORDS

Deep Reactive Ion Etching, loading, microloading, Aspect Ratio Dependent Etching, diffusion, simulation

## INTRODUCTION

### Background

By repeatedly cycling etching and passivation procedures, Deep Reactive Ion Etching (DRIE) enables the fabrication of sophisticated high aspect ratio microstructures on silicon. Each processing cycle can be divided into three consecutive stages [1]: (i) radical-driven, isotropic polymer deposition, (ii) ion-driven, strongly-directional polymer removal, and (iii) a combination of ion-driven (vertical) and radical-driven (isotropic) silicon etching. The polymer/passivation layer prevents the processing of the sidewalls during the etching step of the cycle. In turn, the etching step uses both charged ions and neutral radicals to produce a mixture of both physical (vertical) and chemical (isotropic) etching. The physical component results in an efficient removal of the polymer at the bottom of the structures, as compared to the sidewalls. After this, the substrate is etched by both the vertical and isotropic components, thus restricted to the bottom of the structures. Repetition for many cycles leads to high aspect ratios.

Since the neutrals need to diffuse into the features, the polymer deposition rate and the isotropic component of the silicon etch rate are attenuated with increasing aspect-ratio. However, due to the directional nature of the ion beam, the polymer etch rate is essentially independent of the aspect ratio. Overall, the etch rate per cycle is a complex function of the polymer deposition rate, the polymer etch rate and the silicon etch rate. Thus, the DRIE process is difficult to control/understand and is limited by several side effects.

Microloading refers to the dependence of the overall

etch rate on the density of features [Figure 1(a)]. Equally wide trenches located nearby are etched less deeply than similar trenches located farther apart. As depicted in Figure 1(b), in this study we stress the fact that microloading is due to the development of a lower concentration ( $c$ ) of the etching species at feature-dense areas (e.g.  $c_A < c_A'$ ). This is due to an increased local consumption of the species at the mask level and their slow replacement by diffusional transport from nearby regions.

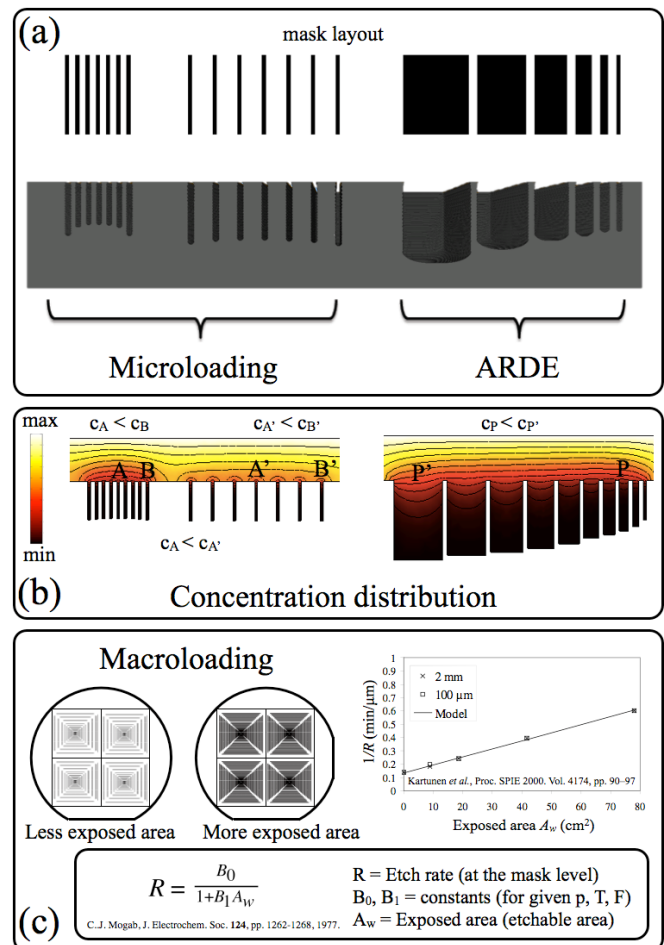


Figure 1: (a) Definition of microloading and ARDE. (b) Local consumption of the etching species leads to lower etchant concentration at feature-dense areas ( $c_A < c_A'$ ) and higher etchant concentration at increasingly wider trenches ( $c_P' > c_P$ ). (c) Etchant consumption and slow transport from regions faraway from the mask level leads to macroloading.

Microloading is related to but different from macroloading. The etch rate is inversely proportional to the total amount of exposed wafer area [Figure 1(c)]. This is due to the consumption of the etchant and its slow transport from regions far above the mask level. Macroloading can be accounted for in simulations by simply correcting the etch rate using the formula shown in Figure 1(c).

In turn, Aspect Ratio Dependent Etching (ARDE) denotes that the etch rate increases with the trench width [Figure 1(a)] and, for a given trench, it decreases with etching time as the aspect ratio increases. We show in this study that also this phenomenon is related to the formation of a concentration distribution across wide/thin trenches (e.g.  $c_p < c_p^*$ ). Ultimately, this is due to a larger consumption of the etching species at the perimeter surface of larger trenches.

### Previous work

In most theoretical models the ions and neutrals reach the silicon surface and react there with etch/deposition rates that are proportional to their flux [2-11], *i.e.* the number of ions/neutrals that arrive per unit time. Thus, a key aspect is to model properly the transport of the ions and neutrals to the surface. The ions are accelerated by the electric field and, thus, they form a beam of vertically-etching particles. Having no charge, however, the neutrals can only diffuse slowly into the etched cavities, where they act as isotropic etching particles.

Considering the source of ions and neutrals as a plane  $P$  right above the sample, there is consensus in the research community that the flux of ions that reaches a given surface point  $\vec{x}$  should be calculated as a visibility integral over the source with a narrow angular distribution of the propagation directions of the ions:

$$F_i(\vec{x}) = \int_P F_i^P \frac{\kappa+1}{2\pi} (\vec{t} \cdot \vec{n}_p)^\kappa \frac{\text{vis}(\vec{x}, \vec{x}_p)(-\vec{t} \cdot \vec{n})}{\|\vec{x} - \vec{x}_p\|^2} dA' \quad (1)$$

where  $\vec{x}_p$  is a point on the source plane  $P$ ,  $F_i^P$  is the ion flux from the source plane,  $\vec{t}$  is the unit vector along the line between  $\vec{x}_p$  and  $\vec{x}$ ,  $\vec{n}$  is the surface normal at  $\vec{x}$ ,  $\vec{n}_p$  is at  $\vec{x}_p$  pointing to the sample,  $\text{vis}(\vec{x}, \vec{x}_p)$  is the visibility function (1 or 0, if the surface points  $\vec{x}$  and  $\vec{x}_p$  are in line of sight or not, respectively) and  $\kappa$  is used to model the narrow angular distribution of the ions, which becomes a normal distribution with standard deviation  $\sigma = 1/\sqrt{\kappa}$  when  $\kappa \gg 1$ . Although Equation (1) is used in Ref. [8], the other studies consider similar expressions, with differences only in the actual form of the angular distribution and/or the dimensionality (2D or 3D).

Having no charge, the neutrals must diffuse randomly into the features of the etch front, typically bouncing several times at the walls until they finally react somewhere. Although the flux of neutrals has been taken to be constant in some studies [2,4,5], there is ample agreement in the research community that thermal diffusive reemission

(independent of the angle of incidence) is essential in order to explain the reduced number of neutrals that reach the bottom of elongated features and, thus, the lag effect. Thus, the flux of neutrals at point  $\vec{x}$  is given by a similar visibility integral over the source and an additional visibility integral over the rest of the surface, to take into account the reemission of the neutrals until they eventually react:

$$F_n(\vec{x}) = \int_P F_n^P \frac{1}{\pi} (\vec{t} \cdot \vec{n}_p) \frac{\text{vis}(\vec{x}, \vec{x}_p)(-\vec{t} \cdot \vec{n})}{\|\vec{x} - \vec{x}_p\|^2} dA' \quad (2)$$

$$+ \int_S F_n(\vec{x}_s) \frac{1}{\pi} (\vec{t} \cdot \vec{n}_s)(1-\theta) \frac{\text{vis}(\vec{x}, \vec{x}_s)(-\vec{t} \cdot \vec{n})}{\|\vec{x} - \vec{x}_s\|^2} dA'$$

where  $\vec{x}_s$  is a point on the surface,  $\vec{n}_s$  is the surface normal at  $\vec{x}_s$  and  $\theta$  is the sticking probability for diffusive re-emission of the neutrals. In practice, this flux is either calculated by conventional integration techniques [6-7] or by Monte Carlo ray-tracing [8], some times using different sticking coefficients at the trench walls and bottom [9-11]. To improve the computational efficiency of the Monte Carlo method, recent reports use a Finite Element approach [11]. This highlights the fact that the use of the visibility integrals is a computationally demanding task.

## DESIGN

### Novelty

Based on the three-stage model [1], our approach deviates markedly from the previous procedures. First of all, regarding the transport of the ions, we focus on the fact that the ion beam is very directional in nature and, thus, few ions are lost at the sidewalls. In other words, the number of ions that reach the bottom of the structures remains essentially the same, even as the depth increases. This is supported by experimental measurements, where the polymer etch rate—due to the ion beam—is essentially independent of the aspect ratio [1]. Correspondingly, we conclude that the vertical component of the silicon etch rate by the ions is essentially constant at any depth.

Secondly, regarding the transport of the radicals, we recognize that the previous models assume Knudsen transport, *i.e.* molecular flow, where collisions between the gas molecules are less frequent than collisions with the surface of the sample. The Knudsen number is the ratio of the mean free path of the molecules to a characteristic length scale of the sample. However, the choice of length scale is not always clear. The etch front itself is evolving and, thus, the system may be in the continuum regime at the start and, perhaps (or not), it may reach the molecular regime after prolonged etching. Therefore, we assume that transport occurs mainly in the continuum regime and, thus, we may focus on solving the differential equation for the concentration of the neutrals.

### Simulation method

Both microloading and ARDE are simultaneously simulated by solving the concentration distribution at every

Bosch cycle and propagating the surface (etching) by considering that the local etch rate is proportional to the actual concentration. We apply the simulation scheme described in Figure 2. At every Bosch cycle, the diffusion equation for the concentration  $c$  of the etching species is solved and, then, etching is performed. Solving  $c$  provides access to its values at the etch front, which are used to determine the etch rate:  $R = a_0 + a_1 \cdot c^b$ . Here,  $a_0$  is the contribution from the ion beam, taken constant at the bottom cells and zero elsewhere, since the accelerated ions are highly directional;  $a_1 \cdot c^b$  is the concentration dependent isotropic contribution from the radicals, since they are neutral and, thus, they diffuse randomly into the cavities.

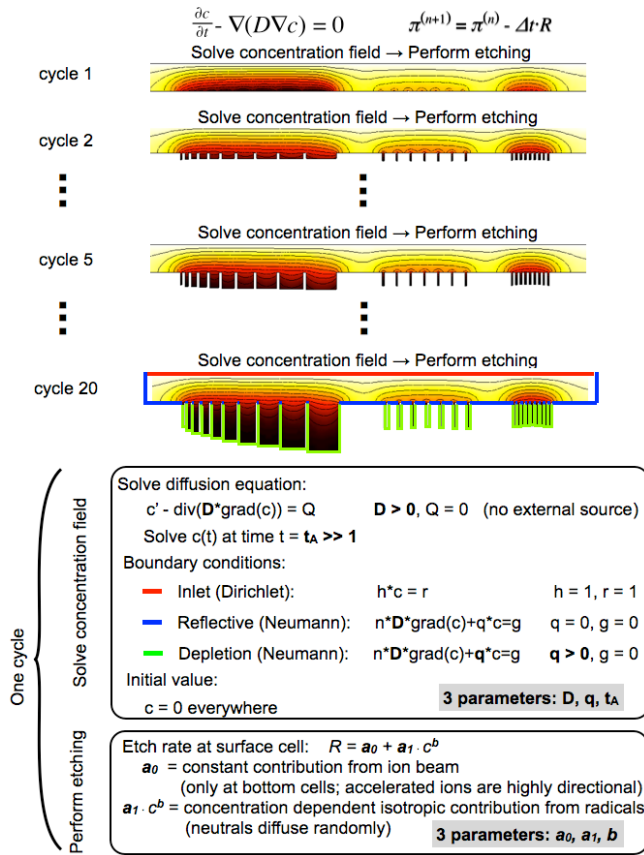


Figure 2: Proposed simulation procedure, consisting in solving the diffusion equation and performing etching at every Bosch cycle, according to the shown details. The diffusion equation for the concentration  $c$  is solved using a finite element method (FEM) continuum description while etching is simulated using a Cellular Automaton (CA).

When solving the diffusion equation, a key aspect is that the etching species should be consumed at the surface perimeter of the trenches (green boundaries in Figure 2). This is obtained by using a depletion term proportional to the concentration at these boundaries ( $n \cdot D \cdot \text{grad}(c) + q \cdot c = 0$  with  $q > 0$ ). Figure 3(a) shows that the incorporation of this depletion results in a concentration distribution that is consistent with ARDE.

The proposed model provides a total of six parameters

in order to describe different experimental conditions and substrates. As an example, Figures 3(b)-(c) show that the concentration distribution can be modeled, realistically affecting the actual depth distribution at the different features.

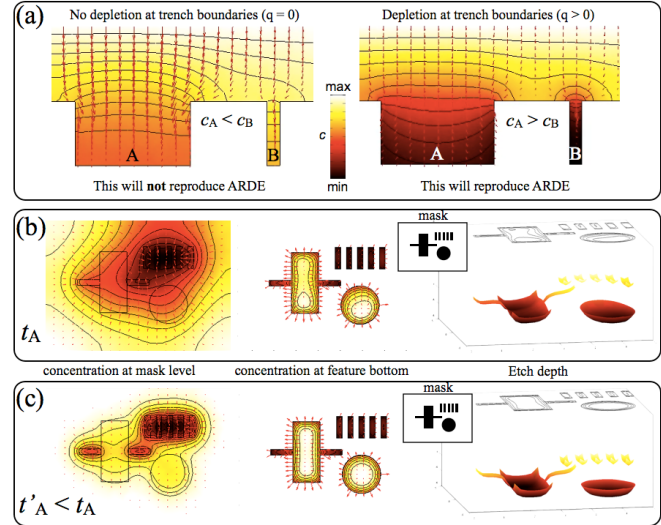


Figure 3: (a) Importance of depletion at trench perimeters. (b-c) Example of dependence of the concentration and depth distributions on model parameter  $t_A$ .

## RESULTS

As shown in Figure 4, the model enables the simultaneous simulation of microloading and ARDE in 3D. Focusing on Figure 4(a), the cross pattern contains both a thick and a thin beam. Cross-section 1 shows that the etch depth is similar at the bottom of the thick beam and circle.

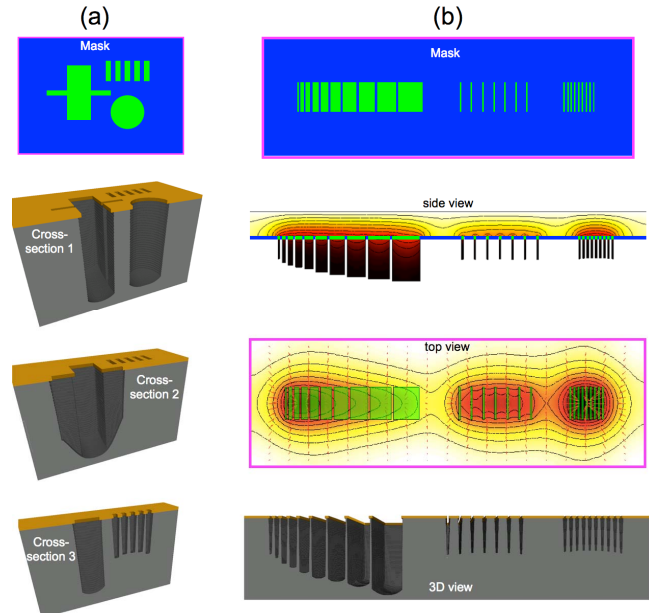


Figure 4: Realistic simulations of DRIE including microloading and ARDE in 3D: (a) Mask pattern and three cross-sections of the resulting structure. (b) Mask pattern, side/top view of the typical concentration distribution of the etching species, and cross-section of an etched structure.

Cross-section 2 shows that the depth at the thin beam has a complex behavior consistent with the lag effect. Finally, cross-section 3 shows that the etch depth at the set of 5 trenches displays a microloading effect and, overall, the depth is smaller than at the circle / thick beam of the cross.

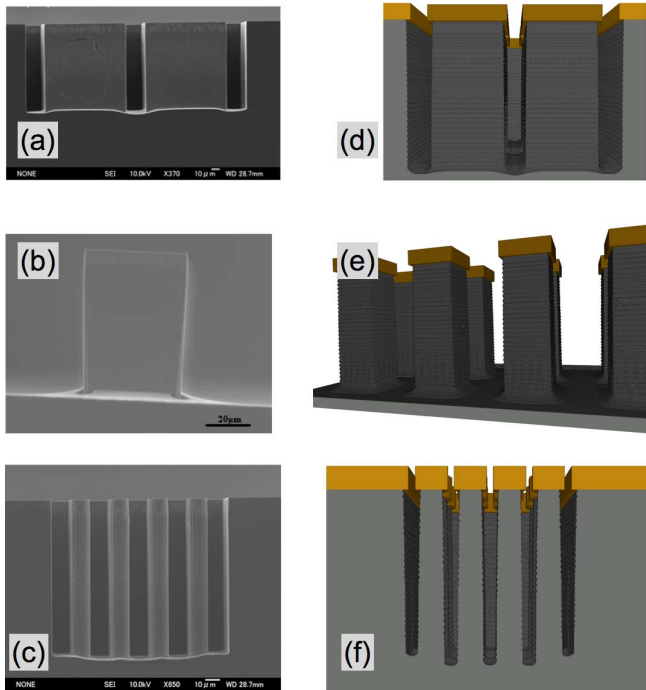


Figure 5: (a)-(c) SEM images of experimental structures [12] and (d)-(f) corresponding simulations including microloading and ARDE.

Figure 5 shows that the simulations compare well with various experiments. In particular, Figures 5(c),(f) show a microloading effect that is opposite to that shown in Figure 4, *i.e.* positive and negative microloading, thus stressing the flexibility of the proposed model.

## CONCLUSION

By deviating from the standard approach to the simulation of DRIE, this study shows that (i) the vertical etching component due to the accelerated ions can be considered to be constant, and (ii) the isotropic etching component due to the neutrals can be modeled using the continuum regime, provided that the etching species is consumed at etched surfaces. The proposed model is rather flexible and is capable of describing the onset of positive/negative microloading and ARDE simultaneously.

## ACKNOWLEDGEMENTS

We are thankful for financial support from: Ramón y Cajal Fellowship Program by the Spanish Ministry of Science and Innovation, ‘Talent’ project by the Chinese state administration of foreign expert affairs (project GDJ 20143201001, Jiangsu Province Talent Human Resource Office, NO.39, 2012), China National High-Tech Research Development Plan 2015AA041804, and National Natural

Science Foundation of China No. 51375093.

## REFERENCES

- [1] S. Lai, D. Johnson and R. Westerman, “Aspect ratio dependent etching lag reduction in deep silicon etch processes”, *J. Vac. Sci. Technol. A*, vol. 24, pp. 1283-1288, 2006.
- [2] R. Zhou, H. Zhang, Y. Hao and Y. Wang, “Simulation of the Bosch process with a string-cell hybrid method”, *J. Micromech. Microeng.*, vol. 14, pp. 851-858, 2004.
- [3] Y. Tan, R. Zhou, H. Zhang and Z. Li, “Modeling and simulation of the lag effect in a deep reactive ion etching process”, *J. Micromech. Microeng.*, vol. 16, pp. 2570–2575, 2006.
- [4] G. Sun, X. Zhao, H. Zhang, L. Wang and Lu G, “3-d simulation of Bosch process with voxel-based method”, *Proc. IEEE NEMS’07 Nano/Micro Engineered and Molecular Systems*, pp. 45-49, 2007.
- [5] F. Zhang, G. Wang, X. Liu, G. Sun, X. Zhao, J. Liu and G. Lu, “An Improved Parallel Implementation of 3-D DRIE Simulation on Multi-core Processors”, *Proc. IEEE HPC’08*, pp. 891-896, 2008.
- [6] T.S. Cale, T.P. Merchant, L.J. Borucki and A.H. Labun, “Topography simulation for the virtual wafer fab”, *Thin Solid Films*, vol. 365, pp. 152-175, 2000.
- [7] G. Kokkoris, A. Tserepi, A.G. Boudouvis and E. Gogolides, “Simulation of SiO<sub>2</sub> and Si feature etching for microelectronics and microelectromechanical systems fabrication: A combined simulator coupling modules of surface etching, local flux calculation, and profile evolution” *J. Vac. Sci. Technol. A*, vol. 22, pp. 1896-1902, 2004.
- [8] O. Ertl and S. Selberherr, “Three-dimensional level set based Bosch process simulations using ray tracing for flux calculation”, *Microelectron. Eng.*, vol. 87, pp. 20-29, 2010.
- [9] B.E. Volland and I.W. Rangelow, “The influence of reactant transport on the profiles of gas chopping etching processes: a simulation approach”, *Microelectron. Eng.*, vol. 67, pp. 338-348, 2003.
- [10] M. Hauguth, T. Danz, B.E. Volland, V. Ishshuk, D. Dreßler and I.W. Rangelow, “New method for the precise flux calculation of neutrals for arbitrary surfaces in profile etch simulations”, *Microelectron. Eng.*, vol. 85, pp. 982-984, 2008.
- [11] V. Ishchuk, B. Volland and I. W. Rangelow, “ViPER: simulation software for high aspect ratio plasma etching of silicon”, *Microsyst. Technol.*, vol. 20, pp. 1791-1796, 2014.
- [12] Y. Li, M. A. Gosálvez, P. Pal, K. Sato and Y. Xing, “Particle Swarm Optimization-based Continuous Cellular Automaton for the simulation of Deep Reactive Ion Etching”, Submitted.

## CONTACT

M.A.G.: +34943015389, miguelangel.gosalvez@ehu.es